ACS OMEGA

http://pubs.acs.org/journal/acsodf

Article

Effects of Chemical Valences of Sulfur on the Performance of CsFAMA Perovskite Solar Cells

Zhenning Xing,[‖] Bing Ou,[‖] Hao Sun, Haipeng Di, Yingrong Jin, Ying Xiong, Feiyi Liao,* and Yiying Zhao*

Cite This: *ACS Omega* 2023, 8, 20912−20919

Read Online

ACCESS | Metrics & More | Article Recommendations | Supporting Information

ABSTRACT: The low electrical conductivity and the high surface defect density of the TiO_2 electron transport layer (ETL) limit the quality of the following perovskite (PVK) layers and the power conversion efficiency (PCE) of corresponding perovskite solar cells (PSCs). Sulfur was reported as an effective element to passivate the TiO_2 layer and improve the PCE of PSCs. In this work, we further investigate the effect of chemical valences of sulfur on the performance of TiO_2/PVK interfaces, CsFAMA PVK layers, and solar cells using TiO_2 ETL layers treated with Na_2S, $Na_2S_2O_3$, and Na_2SO_4, respectively. Experimental results show that the Na_2S and $Na_2S_2O_3$ interfacial layers can enlarge the grain size of PVK layers, reduce the defect density at the TiO_2/PVK interface, and improve the device efficiency and stability. Meanwhile, the Na_2SO_4 interfacial layer leads to a smaller perovskite grain size and a slightly degraded TiO_2/PVK interface and device performance. These results indicate that S^{2-} can obviously improve the quality of TiO_2 and PVK layers and TiO_2/PVK interfaces, while SO_4^{2-} has little effects, even negative effects, on PSCs. This work can deepen the understanding of the interaction between sulfur and the PVK layer and may inspire further progress in the surface passivation field.

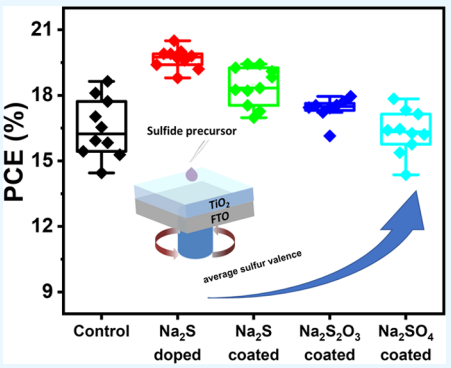

INTRODUCTION

Organic−inorganic halide perovskite semiconductors boost the certified power conversion efficiencies (PCEs) of perovskite solar cells (PSCs) to a new record of 25.7%[1] due to their outstanding optoelectronic properties including excellent light absorption,[2,3] long intrinsic photocarrier diffusion length,[4,5] and high carrier mobility.[6] The PCE losses mainly originate from the charge recombination within the perovskite layers and at the charge transport layer/PVK interfaces, featured as a much shorter carrier lifetime and a higher trap density.[7,8] The quality of the ETL/PVK interfaces has been shown to be detrimental to the performance of perovskite optoelectronic devices.[9]

Organic molecules containing various functional groups were chosen to modify the ETL/PVK interface and reduce the nonradiative recombination. van Reenen et al.[10] showed that a thin [6,6]-phenyl-C_{61}-butyric acid methyl ester (PCBM) layer at the TiO_2/PVK interface could efficiently passivate defects and reduce the hysteresis effect and V_{oc} loss. Wang et al. revealed that the formation of interfacial chemical bonds between PCBM and the SnO_2 layer could be resilient to the removal of DMF in the PVK deposition process, which significantly improved the device performance.[11] Large molecules with Lewis base functional groups, such as self-assembled fullerene derivatives[12,13] pyridine,[14,15] 2-pyridylthiourea,[16] and thiophene,[17,18] were demonstrated to function as an electron donor to passivate the Pb^{2+}-induced traps. However, part of these molecules may dissolve in antisolvents during the preparation of perovskite layers, which limits their applications.[19]

Small molecules with lower cost and better process compatibility were also demonstrated with a similar effect on defect passivation and performance improvement. It has been reported that alkali metal ions such as K^+ and Na^+ and halogen ions such as Cl^-, Br^-, and I^- can modify the electron transport layer and passivate the interface defects, which not only improves the distribution of defects and the binding energy of defects but also promotes interface charge transportation.[20−24] In addition, many sulfur-based additives were introduced to modify the perovskite from different aspects such as controlling nucleation processes,[25] improving phase stability,[26] and stabilizing perovskite precursors.[27] Han[28] et al. demonstrated that the SCN^- ions could coordinate with Pb^{2+} ions in the precursor, leading to the improvement of the stability and reduction of the defect density in PVK layers. You[32] et al. reported that the carboxyl anions, Na^+ ions, and sulfurous acid groups in the heparin sodium could interact with under-

Received: March 13, 2023
Accepted: May 17, 2023
Published: May 27, 2023

ACS Publications

© 2023 The Authors. Published by American Chemical Society

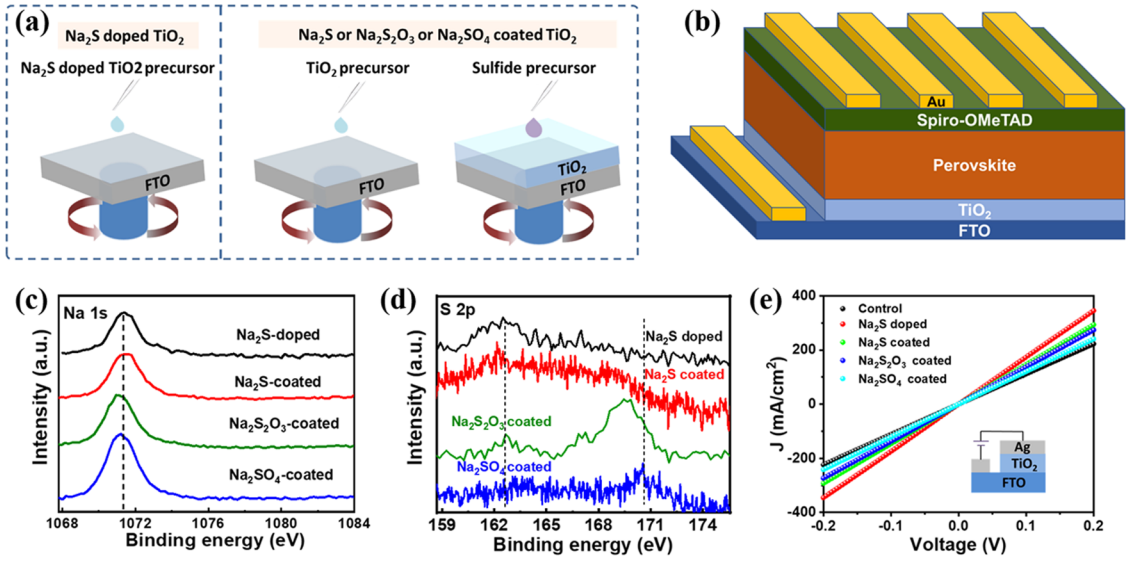

Figure 1. (a) Schematic diagram of the fabrication process of the Na_2S-doped TiO_2 layer (left) and the fabrication process of Na_2S, $Na_2S_2O_3$, and Na_2SO_4-coated TiO_2 layers (right). (b) Device structure of the planar PSCs. (c) Na 1s and (d) S 2p XPS spectra of compact TiO_2 layers treated with Na_2S, $Na_2S_2O_3$, and Na_2SO_4. (e) *I*−*V* characteristics of TiO_2 films treated with different Na_2S, $Na_2S_2O_3$, and Na_2SO_4 sulfides. Inset: device structure for conductivity measurements.

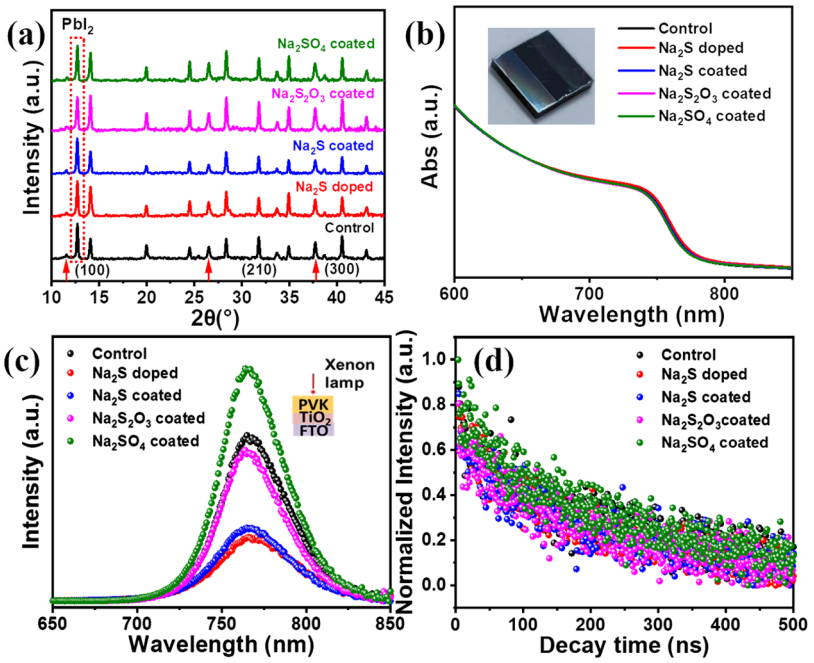

Figure 2. (a) XRD patterns, where the red arrows denote the diffraction peaks of TiO_2, (b) UV−vis spectra (inset: picture of the perovskite film), (c) PL spectra, and (d) TRPL spectra of perovskite films deposited on TiO_2 films treated with Na_2S, $Na_2S_2O_3$, and Na_2SO_4.

coordinated Pb and I ions, resulting in improved PCE. Our previous work showed that the S^{2-}-modified TiO_2 layer could enlarge the grain size and improve the quality of perovskite layers and the PCE.[29−31] However, S^{2-} can be oxidized to high-valence sulfur during actual operation, while none of the above research studies have discussed the effect of sulfur valence on the performance of PSCs. This inspired us to investigate the effects of sulfur valence on the interface modification of TiO_2 layers and the performance of PSCs.

In this work, we investigated the effect of chemical valences of sulfur on the properties of TiO_2 transport layers and the performances of CsMAFA perovskite solar cells using Na_2S, $Na_2S_2O_3$, and Na_2SO_4 solutions to modify the compact TiO_2 substrates. It was found that the Na_2S and $Na_2S_2O_3$ treatment can not only improve the quality of TiO_2/PVK interfaces but also leads to improved PVK morphology and better device performance with average PCEs of 19.62 and 18.40%. However, only a very limited enhancement was found in the Na_2SO_4-treated samples. The effect of average sulfur valence in sulfides was also discussed subsequently. This work will improve the understanding of the effects of sulfur valence on TiO_2-based PSCs and provide references for the selection of interface passivation chemicals.

https://doi.org/10.1021/acsomega.3c01694
ACS Omega 2023, 8, 20912−20919

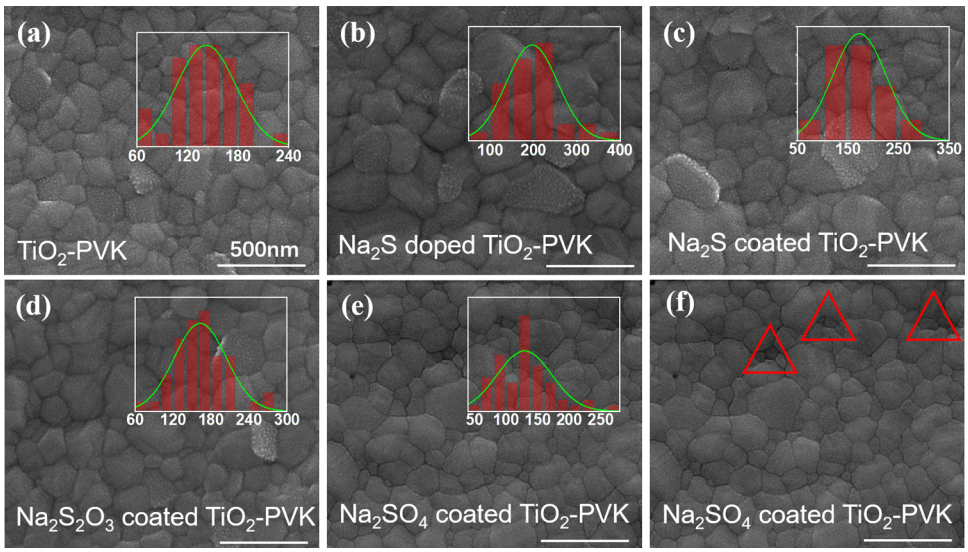

Figure 3. (a)−(e) SEM images of the perovskite films grown on TiO_2 substrates treated with different sulfides and the corresponding grain distribution statistics, where the *x*-axis represents the grain size. The red triangles in (f) stand for the defects of PVK films.

RESULTS AND DISCUSSION

The TiO_2 layers treated with different sulfides were prepared to investigate the chemical valence effect on the properties of the TiO_2 layer and the TiO_2/PVK interface using the process shown in Figure 1a. The corresponding samples were denoted Na_2S-doped, Na_2S-coated, $Na_2S_2O_3$-coated, and Na_2SO_4-coated, respectively. CsFAMA perovskite solar cells with the device structure illustrated in Figure 1b were fabricated to study the chemical valence effect of sulfur on cell performance. The surface chemical states of TiO_2 films treated with different sodium sulfides were characterized by XPS. The XPS peak at 1071.4eV could be identified as Na 1s[33] and found in all TiO_2 films under different treatments, as shown in Figure 1c. The identical Na 1s peak position in four samples confirmed that the four treatment methods could effectively introduce Na elements into TiO_2 films and the chemical states of Na elements were the same. Figure 1d presents the binding energies of S 2p in TiO_2 films treated with different sulfides, where the standard binding energies of S^{2-} (162.8 eV) and S^{6+} (170.3 eV) were marked with two short dashed lines.[33] The S^{2-} peak could be observed in the Na_2S-treated and $Na_2S_2O_3$-treated films separately, indicating the successful introduction of sulfides. Both the S^{2-} peak at 162.8 eV and the S^{6+} peak at 170.3 eV were observed in the XPS spectrum of $Na_2S_2O_3$-treated TiO_2 films, indicating that the sulfur in $Na_2S_2O_3$ is composed of S^{2-} and SO_4^{2-} ions. The peak position of S 2p shifted toward the direction of low binding energy compared with that of S^{6+} in Na_2SO_4, which may be due to the different chemical environments in the samples. In summary, increasing binding energy with an increase of sulfur valence can be observed in XPS measurements.

The *I*−*V* characteristic curves of TiO_2 films treated with four different sulfides were measured to study the influence of sulfur valence on the conductivity of TiO_2 thin films. The device structure for the conductivity measurement and the results are given in Figure 1e. The calculated conductivities of sodium sulfide-treated films were higher than those of controls, which can be attributed to the sodium dopant[34] (Na_2S-doped TiO_2, 5.18 μS/cm; Na_2S spin-coated TiO_2, 4.41 μS/cm; $Na_2S_2O_3$ spin-coated TiO_2, 4.12 μS/cm; Na_2SO_4 spin-coated TiO_2, 3.62 μS/cm; control, 3.35 μS/cm). The conductivity of only Na_2SO_4-coated TiO_2 films showed a small increment, which may have resulted from the compensation of the negative effect of SO_4^{2-} ions on the conductivity of TiO_2 films.

The effects of the chemical valence of sulfur on PVK properties were investigated. The XRD patterns of perovskite films grown on TiO_2 substrates treated with different sulfides are shown in Figure 2a. The diffraction peak surrounded by the red dotted box at 12.7° corresponded to the deliberately introduced PbI_2 in the perovskite films.[35] Meanwhile, three diffraction peaks located at 11.56, 26.52, and 37.71° could be identified as those of the TiO_2 substrate,[36] which were noted with red arrows in Figure 2a. Diffraction peaks of perovskite samples on different substrates are found at the same position in the XRD patterns, indicating that sulfur valance has little effect on the crystallization of perovskite films. The UV−vis absorption spectra of the perovskite films on different substrates showed an absorption edge of 770 nm and were almost identical, as shown in Figure 2b, indicating that the chemical valences of sulfur have little effect on film thicknesses and light absorption properties.

Steady-state photoluminescence (PL) and time-resolved PL (TRPL) measurements are conducted to study the behavior of the photoinduced carrier at the TiO_2/PVK interface on different TiO_2 substrates. As shown in Figure 2c, the PL intensity of the PVK layers on Na_2S-doped, Na_2S-coated, and $Na_2S_2O_3$-coated TiO_2 substrates decreased and that of the PVK layers on the Na_2SO_4-coated TiO_2 substrates increased compared with that of the control samples. The PL intensity increased with the average valence of sulfur in sulfide treatments. The decrease of PL intensity could be attributed to the reduction of radiative recombination and enhanced carrier extraction at the TiO_2/PVK interface. TRPL spectra of PVK layers grown on different TiO_2 substrates are shown in Figure 2d. The fitting transient lifetimes extracted from the spectra of the control, Na_2S-doped, Na_2S-coated, $Na_2S_2O_3$-coated, and the Na_2SO_4-coated samples were 235, 165, 166, 209, and 333 ns, respectively. It could be found that the PVK layers deposited on the TiO_2 substrates treated with Na_2S and $Na_2S_2O_3$ have a shorter carrier lifetime than that of the control, while the lifetime of PVK layers on the TiO_2 substrates treated

https://doi.org/10.1021/acsomega.3c01694
ACS Omega 2023, 8, 20912−20919

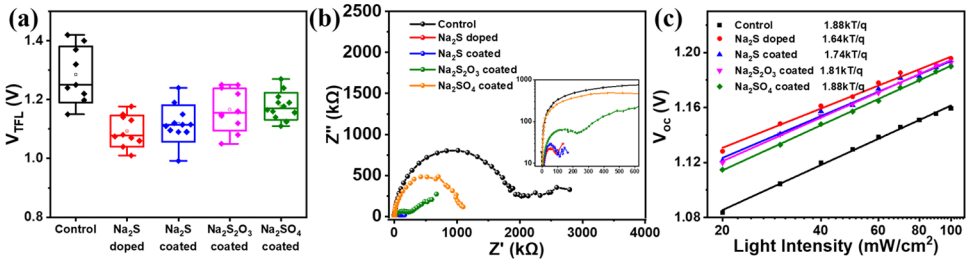

Figure 4. (a) V_{TFL} box diagram of the single-electron devices composed of TiO_2 layers treated with different sulfides. (b) EIS measurements of PSCs composed of TiO_2 layers treated with different sulfides; inset, enlarged region of (b) at a small R_{ct}. (c) Relationship between the optical density and the open-circuit voltage of PSCs composed of TiO_2 films treated with Na_2S, $Na_2S_2O_3$, and Na_2SO_4.

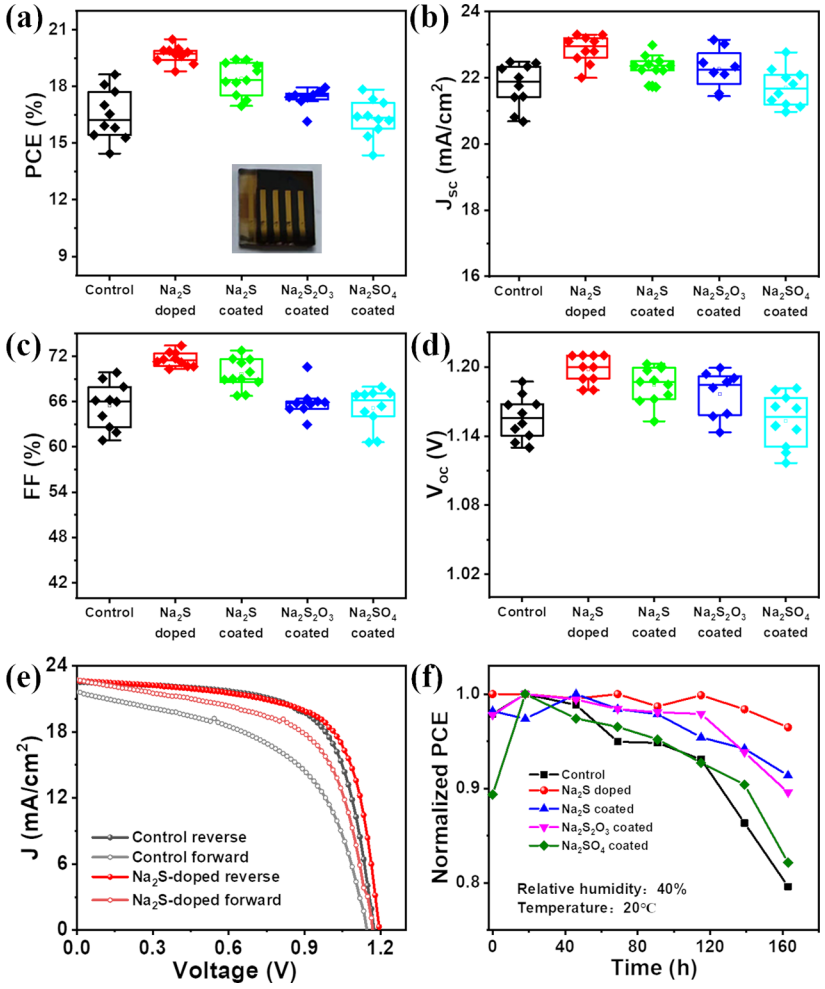

Figure 5. Box diagram of the key performance parameters of PSCs composed of TiO_2 films treated with different sulfides: (a) PCE (inset, photo of PSCs on TiO_2), (b) J_{sc}, (c) FF, and (d) V_{oc}. (e) Reverse and forward $J-V$ curves of the control and Na_2S-doped PSCs. (f) Long-term stability of PSCs composed of TiO_2 layers treated with different sulfides.

with Na_2SO_4 was longer than that of the control. The lifetime increased with an increase of the average valence of sulfur in the sulfide. It could be concluded that the TiO_2 substrates treated with S^{2-} can improve the quality of the TiO_2/PVK interface and the treatment of SO_4^{2-} has a negative effect on the interface.

The SEM images of the PVK layers on different substrates are shown in Figure 3, and the grain size of each sample was calculated to investigate the effects of different sulfide-treated TiO_2 substrates on morphology and grain distribution. The average grain sizes of the control, Na_2S-doped, Na_2S-coated, $Na_2S_2O_3$-coated, Na_2SO_4-coated TiO_2 samples were 142, 196.6, 172.2, 162.3, and 130.5 nm, respectively, corresponding to the peak position fitted with the Gaussian distribution. As shown in Figure 3e, the perovskite films of Na_2S-doped, Na_2S-coated, and $Na_2S_2O_3$-coated samples had larger grain sizes than those of the control, which led to an enhancement of stability and conductivity. The grain sizes of the PVK layers on the Na_2SO_4-coated TiO_2 substrate were smaller than that of the control, which increases the number of grain boundaries of PVK layers and reduces the stability of solar cells. In addition, the SEM image of PVK layers on the Na_2SO_4-coated TiO_2

https://doi.org/10.1021/acsomega.3c01694
ACS Omega 2023, 8, 20912−20919

substrates showed three obvious small defects, which may increase the roughness of the sample and capture carriers. It could be seen that the grain size of perovskite films decreased with increasing chemical valence of sulfur in TiO_2 substrate treatment. The enlargement of the grain size of the PVK layers by S^{2-} ions was consistent with the previous report,[37] and the SO_4^{2-} ions had little, even negative, effect on the quality of PVK layers.

In order to illustrate the effect of TiO_2 substrates treated with different sulfides on the defect state of the PVK layers, we prepared ETL-only devices and conducted space-charge-limited current (SCLC) measurements. The corresponding detailed $J-V$ curves are shown in Figure S1, and the calculated average V_{TFL} values are shown in Figure 4a. The overall trend shows a reduced density of defects in sulfide-treated samples than that in the controls. The defect density of the PVK layers in the Na_2S- and $Na_2S_2O_3$-treated samples was reduced, which could be ascribed to the passivation of S^{2-} ions. The introduced SO_4^{2-} ions can reduce the grain size of PVK layers, as shown in Figure 3, and may induce more defects at the boundaries. The slightly reduced density of defect states in the Na_2SO_4-coated samples may be partially attributed to the passivation effects of Na^+ ions.[38]

EIS measurements were conducted on the cells in a dark environment to investigate the effect of chemical valences of sulfur on the carrier transport capacity at the TiO_2/PVK interface, where R_{ct} can reveal carrier obstruction at the interface. As shown in Figure 4b, R_{ct} values of the control, Na_2S-doped, Na_2S-coated, $Na_2S_2O_3$-coated, and Na_2SO_4-coated samples were 1602, 46, 59, 130, and 900 kΩ, respectively. A smaller R_{ct} value means less radiation recombination of carriers at the interface. The R_{ct} value of the Na_2S-doped sample was the lowest, followed by that of the Na_2S-coated sample, indicating that the doping treatment was better. The R_{ct} value of the $Na_2S_2O_3$-coated sample was relatively large but still much smaller than that of the controls, indicating that $Na_2S_2O_3$ treatment also has a certain improvement effect on the carrier transport at the TiO_2/PVK interface. The R_{ct} value of the Na_2SO_4-coated sample was smaller than that of the control, which may be attributed to the increase of the conductivity of the TiO_2 layers caused by Na^+ ions.

The plot of V_{oc} versus light density in Figure 4c can qualitatively describe the defect density inside the cells and evaluate the overall performance of the devices. Light intensity is proportional to the photogenerated current, and the relationship between the open-circuit voltage and the photocurrent can be described as

$$V_{oc} = \frac{nkT}{q} \ln\left(\frac{I_{ph}}{I_0} + 1\right)$$

where n is the ideal factor, k is the Boltzmann constant, T is the absolute temperature, I_{ph} is the photogenerated current, I_0 is the reverse saturation current, and q is the electronic charge. The calculated n values of samples were 1.88 (control), 1.64 (Na_2S-doped), 1.74 (Na_2S-coated), 1.81 ($Na_2S_2O_3$-coated), and 1.88 (Na_2SO_4-coated), which positively corelates with the defect density. The defect density of the Na_2S- and $Na_2S_2O_3$-treated samples decreased obviously, while that of the Na_2SO_4-treated samples was the same as that of the controls, which is consistent with the SCLC measurement results of the ETL-only devices.

To further study the effect of sulfur valences on device performance, classic planar solar cells (FTO/TiO_2/sulfides/PVK/Spiro-OMeTAD/Au) were prepared with different sodium sulfide treatments. Ten solar cells for each type of substrate were measured under AM 1.5 G (100 mW cm^{-2})-simulated solar illumination conditions, and the corresponding statistic diagram are presented in Figure 5a–d. As shown in Figure 5a, the average PCEs of cells on the Na_2S-doped, Na_2S-coated, and $Na_2S_2O_3$-coated TiO_2 substrates considerably improved from 16.25% to 19.62%, 18.40%, and 17.47%, respectively, while the average PCE of the Na_2SO_4-coated TiO_2 substrate was around 16.33%, suggesting that the SO_4^{2-} ions have different effects on the devices. Similar trends could be found for the parameters of V_{oc}, FF, and J_{sc}. It could be concluded that S^{2-} ions had a positive effect on device efficiency, while the SO_4^{2-} ions had little, even negative, effects. The introduction of S^{2-} greatly enhanced the J_{sc}, which was consistent with the decrease of the PL intensity and luminescence lifetime shown in Figure 2 and the improvement of EQE values in Figure S2f. This indicated that the introduction of S^{2-} ions can reduce the recombination of carriers and enhance the extraction capacity of carriers at the TiO_2/PVK interface. However, the J_{sc} of Na_2SO_4-coated devices was lower than that of the controls, indicating that SO_4^{2-} deteriorates the TiO_2/PVK interface and slightly degrades the device performance.

Figure 5e shows the reverse and forward sweep $J-V$ curves of the control sample and the Na_2S-doped sample, and the remaining results are presented in Figure S2. The control sample gave an obvious hysteresis from the reverse to the forward scans, while the Na_2S-doped one showed a marked reduction of the hysteresis, resulting in an improvement of the electrical conductivity of the TiO_2 layer and a reduced interface carrier recombination of the TiO_2/PVK interface. As expected, the Na_2SO_4-doped sample showed little improvement in the hysteresis due to the poor effect of SO_4^{2-} on the interface.

We further explored the effect of different sulfide treatments on the performance stability of unencapsulated solar cells. As excepted, the samples treated with lower-valence sulfide demonstrated better long-term air stability, as shown in Figure 5f. The Na_2S-doped sample could still maintain 96.5% of the initial PCE after 163 h of exposure in the air condition, 91.4% for the Na_2S-coated sample, 89.6% for the $Na_2S_2O_3$-coated sample, 82.1% for the Na_2SO_4-coated sample, while only 79.6% for the control sample. The stability of the cells improved after the introduction of Na_2S and $Na_2S_2O_3$ into the TiO_2 layer, while the stability did not improve after the introduction of Na_2SO_4. This is consistent with the previous experimental results that the S^{2-} ions have obvious improvement effects on the TiO_2/PVK interfaces and the PVK layers, while SO_4^{2-} ions have little effect on the interface and the PVK layer. The slight improvement in the performance of Na_2SO_4-coated samples could be attributed to the increase of conductivity of TiO_2 layers by Na^+ ions.

CONCLUSIONS

In summary, we adopted sulfides with different chemical valences to modify the TiO_2 layer and investigated their impacts on the properties of the TiO_2/PVK interfaces and PVK layers and the performance of corresponding CsFAMA solar cells. The Na_2S- and $Na_2S_2O_3$-treated TiO_2 layers could enhance the carrier extraction capacity at the TiO_2/PVK

https://doi.org/10.1021/acsomega.3c01694
ACS Omega 2023, 8, 20912−20919

interface due to the introduction of Na^+ and S^{2-}. The Na_2S- and $Na_2S_2O_3$-treated TiO_2 layers led to the improved crystal quality of the PVK layers in terms of grain size, reduced defect density and dark current, and improved hysteresis effect and device stability. Meanwhile, Na_2SO_4-modified TiO_2 layers had no significant effect on the carrier extraction ability at the TiO_2/PVK interface and even negative effects on the morphology of the following PVK layers. As a result, the cell performance showed a slight improvement compared with the control sample. This work may provide insights into choosing sulfides and proper chemical valences to modify the TiO_2/PVK interfaces.

EXPERIMENTAL SECTION

Solution Preparation. The pure TiO_2 precursors were prepared by dissolving tetrabutyl titanate (250 μL, Sigma-Aldrich) and hydrochloric acid (25 μL, Kelong) in absolute ethyl alcohol (3 mL, Aladdin). For Na_2S-doped TiO_2 precursors, absolute ethyl alcohol (Aladdin)-dissolved anhydrous Na_2S (Aladdin), according to the molar ratio of Na_2S and TiO_2, was added into the preparedpure TiO_2 precursors. The sulfide coating precursors were prepared by dissolving different sulfides (Na_2S (Aladdin), $Na_2S_2O_3$ (Aladdin), and Na_2SO_4 (Aladdin)) in absolute ethyl alcohol (Aladdin) according to the concentration of sulfides. The $Cs_{0.1}(MA_{0.15}FA_{0.85})_{0.9}Pb(Br_{0.15}I_{0.85})_3$ precursors were prepared by mixing five components in 700 μL of DMF and 300 μL of DMSO according to the proportion. The components consisted of cesium iodide (CsI, 31.2 mg, Alfa Aesra), methylammonium bromide (MABr, 18.1 mg, lumtec), lead bromide ($PbBr_2$, 66.1 mg, Sigma-Aldrich), formamidinium iodide (FAI, 157.9 mg, luminescence), and lead iodide (PbI_2, 470.2 mg, Sigma-Aldrich). The Spiro-OMeTAD solutions were prepared by mixing chlorobenzene (1 mL, Alfa Aesar)-dissolved 2,2′,7,7′-tetrakis[*N*,*N*-di(4-methoxyphenyl)amino]-9,9′-spirobifluorene (Spiro, 72.3 mg, luminescence), 4-tert-butylpyridine (28.8 μL, Sigma-Aldrich), and Li-TFSI solution 17.5 μL, Li-TFSI (520 mg, Sigma-Aldrich) in acetonitrile (1 mL, Alfa Aesar) and Co(III) TFSI salt solution (60 μL, FK209 Co(III) TFSI salt (100 mg, luminescence) in chlorobenzene (1 mL, Alfa Aesar)). Both perovskite precursors and Spiro-OMeTAD solutions should be kept in a glovebox overnight at room temperature. PCBM (20 mg, Baolaite Industrial Co.) was dissolved in acetonitrile (1 mL, Alfa Aesar).

Device Fabrication. The FTO glass (sheet resistance = 7 Ω sq^{-1}) was sequentially cleaned with detergent, deionized water, acetone, and ethyl alcohol in an ultrasonicator for 20 min, then dried with a nitrogen gun, and treated by plasma cleaning for 15 min. The TiO_2- or Na_2S-doped TiO_2 compact layers were prepared by spin coating the TiO_2- or Na_2S-doped TiO_2 precursor solution onto the FTO substrates at 5000 rpm for 30 s in the air. Then, the samples were preannealed at 120 °C for 20 min on a hot plate and heated in a muffle oven at 450 °C for 1 h to form the c-TiO_2 layers. For the Na_2S-, $Na_2S_2O_3$-, or Na_2SO_4-coated samples, the corresponding precursor solutions were spin-coated onto the compact TiO_2 layers at 5000 rpm for 30 s in the air and annealed at 120 °C for 20 min on the hot plate to form the interfacial layers. Samples were treated with plasma cleaning for 15 min before the PVK deposition process and then transferred into a glovebox. PVK layers were deposited rapidly by a one-step spin coating process at 500 rpm for 5s and 5000 rpm for 50 s on FTO/c-TiO_2 substrates, and 50 μL of chlorobenzene (Alfa Aesar) was injected onto the spinning substrate constantly. All samples were then annealed at 150 °C for 10 min covered with a Petri dish. The Spiro-OMeTAD precursor was then deposited on PVK layers by spin coating at 5000 rpm for 50 s. At last, 80 nm thick Au electrodes were deposited on the devices by vacuum thermal evaporation.

Characterization. The $I-V$ measurements and stability tests were performed on a Keithley 2400 digital source meter under simulated sunlight from a Newport 94123A solar simulator matching the AM 1.5G irradiation (100 mW cm^{-2}). The devices were measured from 1.4 to −0.2 V at a scan rate of 10 mV/s. X-ray photoelectron spectroscopy (XPS) was carried out on a PHI 5000 Versa Probe III. UV−vis absorption spectra were recorded with a Youke UV-1901 UV-vis spectrometer. SCLC and conductivity were tested on a Keithley 2400 digital source meter. SEM images were recorded on a field-emission scanning electron microscopy (FEI inspect) instrument at an acceleration voltage of 8 kV. Steady-state photoluminescence (PL) and time-resolved PL (TRPL) spectra were recorded using an Edinburgh Instruments FLS 980 equipped with a light source with an excitation wavelength of 375 nm. EIS plots were constructed on a CorrTest Electrochemical Workstation under dark conditions.

The formula for calculating the conductivity of the TiO_2 substrates can be described as

$$\sigma = ID(AV)^{-1}$$

where σ is the conductivity of the sample, I and V are the measured current and voltage, respectively, A is the area of the measured sample, which is 5.5 mm^2, and D represents the thickness of the TiO_2 layer, which is 30 nm for each sample.

ASSOCIATED CONTENT

Supporting Information

The Supporting Information is available free of charge at https://pubs.acs.org/doi/10.1021/acsomega.3c01694.

Dark $J-V$ characteristic curves of the single-electron devices, reverse and forward $J-V$ curves, and EQE measurement of solar cells (PDF)

AUTHOR INFORMATION

Corresponding Authors

Feiyi Liao − *Institute of Materials, China Academy of Engineering Physics, Jiangyou 621908, China; State Key Laboratory of Environment-friendly Energy Materials, Southwest University of Science and Technology, Mianyang 621010, China*; Email: david3349@163.com

Yiying Zhao − *Institute of Materials, China Academy of Engineering Physics, Jiangyou 621908, China*; orcid.org/0000-0002-1424-2516; Email: zhaoyiying@caep.cn

Authors

Zhenning Xing − *Institute of Materials, China Academy of Engineering Physics, Jiangyou 621908, China*

Bing Ou − *Institute of Materials, China Academy of Engineering Physics, Jiangyou 621908, China; School of Materials Science and Engineering, Xihua University, Chengdu 610039, China*

Hao Sun − *Institute of Materials, China Academy of Engineering Physics, Jiangyou 621908, China*

Haipeng Di − *Institute of Materials, China Academy of Engineering Physics, Jiangyou 621908, China*

https://doi.org/10.1021/acsomega.3c01694
ACS Omega 2023, 8, 20912−20919

Yingrong Jin − *School of Materials Science and Engineering, Xihua University, Chengdu 610039, China*
Ying Xiong − *State Key Laboratory of Environment-friendly Energy Materials, Southwest University of Science and Technology, Mianyang 621010, China*

Complete contact information is available at: https://pubs.acs.org/10.1021/acsomega.3c01694

Author Contributions

∥Z.X. and B.O. contributed equally to this work.

Notes

The authors declare no competing financial interest.

■ ACKNOWLEDGMENTS

This study received fundamental research funds from the Sichuan Science and Technology Program (No. 2021JDTD0021 and 2022ZYD0015), the Innovation Funds from China Academy of Engineering Physics (No. CX20210037), and the Open Project of the State Key Laboratory of Environment-friendly Energy Materials (No. 21kfhg04).

■ REFERENCES

(1) National Renewable Energy Laboratory (NREL). Best Research-Cell Efficiency Chart|Photovoltaic Research|NREL. https://www.nrel.gov/pv/cell-efficiency.html (accessed Jan 10, 2023).
(2) De Roo, J.; Ibáñez, M.; Geiregat, P.; Nedelcu, G.; Walravens, W.; Maes, J.; Martins, J. C.; Van Driessche, I.; Kovalenko, M. V.; Hens, Z. Highly Dynamic Ligand Binding and Light Absorption Coefficient of Cesium Lead Bromide Perovskite Nanocrystals. *ACS Nano* **2016**, *10*, 2071−2081.
(3) Shen, Q.; Ogomi, Y.; Chang, J.; Toyoda, T.; Fujiwara, K.; Yoshino, K.; Sato, K.; Yamazaki, K.; Akimoto, M.; Kuga, Y.; Katayama, K.; Hayase, S. Optical Absorption, Charge Separation and Recombination Dynamics in Sn/Pb Cocktail Perovskite Solar Cells and Their Relationships to Photovoltaic Performances. *J. Mater. Chem. A* **2015**, *3*, 9308−9316.
(4) Zhumekenov, A. A.; Saidaminov, M. I.; Haque, M. A.; Alarousu, E.; Sarmah, S. P.; Murali, B.; Dursun, I.; Miao, X.-H.; Abdelhady, A. L.; Wu, T.; Mohammed, O. F.; Bakr, O. M. Formamidinium Lead Halide Perovskite Crystals with Unprecedented Long Carrier Dynamics and Diffusion Length. *ACS Energy Lett.* **2016**, *1*, 32−37.
(5) Wu, B.; Zhou, Y.; Xing, G.; Xu, Q.; Garces, H. F.; Solanki, A.; Goh, T. W.; Padture, N. P.; Sum, T. C. Long Minority-Carrier Diffusion Length and Low Surface-Recombination Velocity in Inorganic Lead-Free CsSnI3 Perovskite Crystal for Solar Cells. *Adv. Funct. Mater.* **2017**, *27*, 1604818.
(6) Dong, Q.; Fang, Y.; Shao, Y.; Mulligan, P.; Qiu, J.; Cao, L.; Huang, J. Electron-Hole Diffusion Lengths > 175 Mm in Solution-Grown CH3NH3PbI3 Single Crystals. *Science* **2015**, *347*, 967−970.
(7) Chen, B.; Rudd, P. N.; Yang, S.; Yuan, Y.; Huang, J. Imperfections and Their Passivation in Halide Perovskite Solar Cells. *Chem. Soc. Rev.* **2019**, *48*, 3842−3867.
(8) Wolff, C. M.; Caprioglio, P.; Stolterfoht, M.; Neher, D. Nonradiative Recombination in Perovskite Solar Cells: The Role of Interfaces. *Adv. Mater.* **2019**, *31*, No. 1902762.
(9) Chen, J.; Park, N.-G. Causes and Solutions of Recombination in Perovskite Solar Cells. *Adv. Mater.* **2019**, *31*, No. 1803019.
(10) van Reenen, S.; Kemerink, M.; Snaith, H. J. Modeling Anomalous Hysteresis in Perovskite Solar Cells. *J. Phys. Chem. Lett.* **2015**, *6*, 3808−3814.
(11) Wang, J.; Datta, K.; Weijtens, C. H. L.; Wienk, M. M.; Janssen, R. A. J. Insights into Fullerene Passivation of SnO2 Electron Transport Layers in Perovskite Solar Cells. *Adv. Funct. Mater.* **2019**, *29*, No. 1905883.
(12) Zhou, W.; Zhen, J.; Liu, Q.; Fang, Z.; Li, D.; Zhou, P.; Chen, T.; Yang, S. Successive Surface Engineering of TiO2 Compact Layers via Dual Modification of Fullerene Derivatives Affording Hysteresis-Suppressed High-Performance Perovskite Solar Cells. *J. Mater. Chem. A* **2017**, *5*, 1724−1733.
(13) Cai, F.; Yang, L.; Yan, Y.; Zhang, J.; Qin, F.; Liu, D.; Cheng, Y.-B.; Zhou, Y.; Wang, T. Eliminated Hysteresis and Stabilized Power Output over 20% in Planar Heterojunction Perovskite Solar Cells by Compositional and Surface Modifications to the Low-Temperature-Processed TiO2 Layer. *J. Mater. Chem. A* **2017**, *5*, 9402−9411.
(14) Nagaoka, H.; Ma, F.; deQuilettes, D. W.; Vorpahl, S. M.; Glaz, M. S.; Colbert, A. E.; Ziffer, M. E.; Ginger, D. S. Zr Incorporation into TiO2 Electrodes Reduces Hysteresis and Improves Performance in Hybrid Perovskite Solar Cells While Increasing Carrier Lifetimes. *J. Phys. Chem. Lett.* **2015**, *6*, 669−675.
(15) Zeng, Q.; Zhang, X.; Feng, X.; Lu, S.; Chen, Z.; Yong, X.; Redfern, S. A. T.; Wei, H.; Wang, H.; Shen, H.; Zhang, W.; Zheng, W.; Zhang, H.; Tse, J. S.; Yang, B. Polymer-Passivated Inorganic Cesium Lead Mixed-Halide Perovskites for Stable and Efficient Solar Cells with High Open-Circuit Voltage over 1.3 V. *Adv. Mater.* **2018**, *30*, No. 1705393.
(16) Sun, M.; Zhang, F.; Liu, H.; Li, X.; Xiao, Y.; Wang, S. Tuning the Crystal Growth of Perovskite Thin-Films by Adding the 2-Pyridylthiourea Additive for Highly Efficient and Stable Solar Cells Prepared in Ambient Air. *J. Mater. Chem. A* **2017**, *5*, 13448−13456.
(17) Meng, L.; Sun, C.; Wang, R.; Huang, W.; Zhao, Z.; Sun, P.; Huang, T.; Xue, J.; Lee, J.-W.; Zhu, C.; Huang, Y.; Li, Y.; Yang, Y. Tailored Phase Conversion under Conjugated Polymer Enables Thermally Stable Perovskite Solar Cells with Efficiency Exceeding 21%. *J. Am. Chem. Soc.* **2018**, *140*, 17255−17262.
(18) Wen, T. Y.; Yang, S.; Liu, P. F.; Tang, L. J.; Qiao, H. W.; Chen, X.; Yang, X. H.; Hou, Y.; Yang, H. G. Surface Electronic Modification of Perovskite Thin Film with Water-Resistant Electron Delocalized Molecules for Stable and Efficient Photovoltaics. *Adv. Energy Mater.* **2018**, *8*, No. 1703143.
(19) Wang, Y.; Liu, J.; Yu, M.; Zhong, J.; Zhou, Q.; Qiu, J.; Zhang, X. SnO2 Surface Halogenation to Improve Photovoltaic Performance of Perovskite Solar Cells. *Acta Phys. Chim. Sin.* **2021**, No. 2006030.
(20) Abdi-Jalebi, M.; Andaji-Garmaroudi, Z.; Cacovich, S.; Stavrakas, C.; Philippe, B.; Richter, J. M.; Alsari, M.; Booker, E. P.; Hutter, E. M.; Pearson, A. J.; Lilliu, S.; Savenije, T. J.; Rensmo, H.; Divitini, G.; Ducati, C.; Friend, R. H.; Stranks, S. D. Maximizing and Stabilizing Luminescence from Halide Perovskites with Potassium Passivation. *Nature* **2018**, *555*, 497−501.
(21) Bi, C.; Zheng, X.; Chen, B.; Wei, H.; Huang, J. Spontaneous Passivation of Hybrid Perovskite by Sodium Ions from Glass Substrates: Mysterious Enhancement of Device Efficiency Revealed. *ACS Energy Lett.* **2017**, *2*, 1400−1406.
(22) Liu, X.; Zhang, Y.; Shi, L.; Liu, Z.; Huang, J.; Yun, J. S.; Zeng, Y.; Pu, A.; Sun, K.; Hameiri, Z.; Stride, J. A.; Seidel, J.; Green, M. A.; Hao, X. Exploring Inorganic Binary Alkaline Halide to Passivate Defects in Low-Temperature-Processed Planar-Structure Hybrid Perovskite Solar Cells. *Adv. Energy Mater.* **2018**, *8*, No. 1800138.
(23) Wang, Z.; Zhou, Y.; Pang, S.; Xiao, Z.; Zhang, J.; Chai, W.; Xu, H.; Liu, Z.; Padture, N. P.; Cui, G. Additive-Modulated Evolution of HC(NH2)2PbI3 Black Polymorph for Mesoscopic Perovskite Solar Cells. *Chem. Mater.* **2015**, *27*, 7149−7155.
(24) Son, D.-Y.; Lee, J.-W.; Choi, Y. J.; Jang, I.-H.; Lee, S.; Yoo, P. J.; Shin, H.; Ahn, N.; Choi, M.; Kim, D.; Park, N.-G. Self-Formed Grain Boundary Healing Layer for Highly e Cient CH3NH3PbI3 Perovskite Solar Cells. *Nat. ENERGY* **2016**, *1*, 16081.
(25) Zhou, T.; Lai, H.; Liu, T.; Lu, D.; Wan, X.; Zhang, X.; Liu, Y.; Chen, Y. Highly Efficient and Stable Solar Cells Based on Crystalline Oriented 2D/3D Hybrid Perovskite. *Adv. Mater.* **2019**, 1901242.
(26) Leblanc, A.; Mercier, N.; Allain, M.; Dittmer, J.; Pauporté, T.; Fernandez, V.; Boucher, F.; Kepenekian, M.; Katan, C. Enhanced Stability and Band Gap Tuning of α-[HC(NH$_2$)$_2$]PbI$_3$ Hybrid Perovskite by Large Cation Integration. *ACS Appl. Mater. Interfaces* **2019**, *11*, 20743−20751.

(27) Zhou, Y.; Liu, C.; Meng, F.; Zhang, C.; Wei, G.; Gao, L.; Ma, T. Recent Progress in Perovskite Solar Cells Modified by Sulfur Compounds. *Sol. RRL* **2021**, *5*, No. 2000713.
(28) Han, Q.; Bai, Y.; Liu, J.; Du, K.; Li, T.; Ji, D.; Zhou, Y.; Cao, C.; Shin, D.; Ding, J.; Franklin, A. D.; Glass, J. T.; Hu, J.; Therien, M. J.; Liu, J.; Mitzi, D. B. Additive Engineering for High-Performance Room-Temperature-Processed Perovskite Absorbers with Micron-Size Grains and Microsecond-Range Carrier Lifetimes. *Energy Environ. Sci.* **2017**, *10*, 2365−2371.
(29) Sun, H.; Xie, D.; Song, Z.; Liang, C.; Xu, L.; Qu, X.; Yao, Y.; Li, D.; Zhai, H.; Zheng, K.; Cui, C.; Zhao, Y. Interface Defects Passivation and Conductivity Improvement in Planar Perovskite Solar Cells Using Na2S-Doped Compact TiO2 Electron Transport Layers. *Acs Appl. Mater. Interfaces* **2020**, *12*, 22853−22861.
(30) Liu, Y.; Sun, H.; Liao, F.; Li, G.; Zhao, C.; Cui, C.; Mei, J.; Zhao, Y. Bridging Effects of Sulfur Anions at Titanium Oxide and Perovskite Interfaces on Interfacial Defect Passivation and Performance Enhancement of Perovskite Solar Cells. *ACS Omega* **2021**, *6*, 34485−34493.
(31) Ou, B.; Liu, Y.; Sun, H.; Xing, Z.; Di, H.; Jin, Y.; Zhao, Y. Understanding the Working Mechanism of S2− Ions on Compacted TiO2 Layers in Cesium−Methylammonium−Formamidinium Perovskite Solar Cells. *ACS Appl. Energy Mater.* **2022**, *5*, 13377−13384.
(32) You, S.; Wang, H.; Bi, S.; Zhou, J.; Qin, L.; Qiu, X.; Zhao, Z.; Xu, Y.; Zhang, Y.; Shi, X.; Zhou, H.; Tang, Z. A Biopolymer Heparin Sodium Interlayer Anchoring TiO2 and MAPbI(3) Enhances Trap Passivation and Device Stability in Perovskite Solar Cells. *Adv. Mater.* **2018**, *30*, No. 1706924.
(33) NIST X-ray Photoelectron Spectroscopy Database. *NIST Standard Reference Database Number 20*; National Institute of Standards and Technology: Gaithersburg MD, 2000.
(34) Li, X.; Yang, J.; Jiang, Q.; Chu, W.; Zhang, D.; Zhou, Z.; Xin, J. Synergistic Effect to High-Performance Perovskite Solar Cells with Reduced Hysteresis and Improved Stability by the Introduction of Na-Treated TiO2 and Spraying-Deposited CuI as Transport Layers. *ACS Appl. Mater. Interfaces* **2017**, *9*, 41354−41362.
(35) Chen, Q.; Zhou, H.; Song, T.-B.; Luo, S.; Hong, Z.; Duan, H.-S.; Dou, L.; Liu, Y.; Yang, Y. Controllable Self-Induced Passivation of Hybrid Lead Iodide Perovskites toward High Performance Solar Cells. *Nano Lett.* **2014**, *14*, 4158−4163.
(36) Chen, P.; Bai, Y.; Wang, S.; Lyu, M.; Yun, J.-H.; Wang, L. In Situ Growth of 2D Perovskite Capping Layer for Stable and Efficient Perovskite Solar Cells. *Adv. Funct. Mater.* **2018**, *28*, No. 1706923.
(37) Sun, H.; Xie, D.; Song, Z.; Liang, C.; Xu, L.; Qu, X.; Yao, Y.; Li, D.; Zhai, H.; Zheng, K.; Cui, C.; Zhao, Y. Interface Defects Passivation and Conductivity Improvement in Planar Perovskite Solar Cells Using Na_2 S-Doped Compact TiO_2 Electron Transport Layers. *ACS Appl. Mater. Interfaces* **2020**, *12*, 22853−22861.
(38) Bi, C.; Zheng, X.; Chen, B.; Wei, H.; Huang, J. Spontaneous Passivation of Hybrid Perovskite by Sodium Ions from Glass Substrates: Mysterious Enhancement of Device Efficiency Revealed. *ACS Energy Lett.* **2017**, *2*, 1400−1406.

https://doi.org/10.1021/acsomega.3c01694
ACS Omega 2023, 8, 20912−20919